STEM CELLS

TISSUE-SPECIFIC STEM CELLS

Purinergic and Store-Operated Ca^{2+} Signaling Mechanisms in Mesenchymal Stem Cells and Their Roles in ATP-Induced Stimulation of Cell Migration

HONGSEN PENG,[a,b] YUNJIE HAO,[a] FATEMA MOUSAWI,[a] SEBASTIEN ROGER,[c] JING LI,[a] JOAN A. SIM,[d] SREENIVASAN PONNAMBALAM,[e] XUEBIN YANG,[b] LIN-HUA JIANG[a,f]

Key Words.

ABSTRACT

ATP is an extrinsic signal that can induce an increase in the cytosolic Ca^{2+} level ($[Ca^{2+}]_c$) in mesenchymal stem cells (MSCs). However, the cognate intrinsic mechanisms underlying ATP-induced Ca^{2+} signaling in MSCs is still contentious, and their importance in MSC migration remains unknown. In this study, we investigated the molecular mechanisms underlying ATP-induced Ca^{2+} signaling and their roles in the regulation of cell migration in human dental pulp MSCs (hDP-MSCs). RT-PCR analysis of mRNA transcripts and interrogation of agonist-induced increases in the $[Ca^{2+}]_c$ support that P2X7, $P2Y_1$, and $P2Y_{11}$ receptors participate in ATP-induced Ca^{2+} signaling. In addition, following P2Y receptor activation, Ca^{2+} release-activated Ca^{2+} Orai1/Stim1 channel as a downstream mechanism also plays a significant role in ATP-induced Ca^{2+} signaling. ATP concentration-dependently stimulates hDP-MSC migration. Pharmacological and genetic interventions of the expression or function of the P2X7, $P2Y_1$ and $P2Y_{11}$ receptors, and Orai1/Stim1 channel support critical involvement of these Ca^{2+} signaling mechanisms in ATP-induced stimulation of hDP-MSC migration. Taken together, this study provide evidence to show that purinergic P2X7, $P2Y_1$, and $P2Y_{11}$ receptors and store-operated Orai1/Stim1 channel represent important molecular mechanisms responsible for ATP-induced Ca^{2+} signaling in hDP-MSCs and activation of these mechanisms stimulates hDP-MSC migration. Such information is useful in building a mechanistic understanding of MSC homing in tissue homeostasis and developing more efficient MSC-based therapeutic applications. STEM CELLS *2016;34:2102–2114*

SIGNIFICANCE STATEMENT

ATP is an important signaling molecule that regulates diverse cell functions. Mesenchymal stem cells (MSCs) have promising potential of therapeutic application but the migration capacity of MSCs limits the effectiveness of MSC-based therapies. MSCs release ATP and here we provide evidence to show that ATP stimulates MSC migration through purinergic P2X7, $P2Y_1$, and $P2Y_{11}$ receptors. Our study is the first to find that Orai1 and Sitm1 form Ca^{2+}-release-activated-Ca^{2+} channel as downstream Ca^{2+} signaling mechanism mediating ATP-induced stimulation of MSC migration. These results reveal novel mechanisms regulating MSC migration. Such information is desirable in optimization of MSC cultures for therapeutic use.

INTRODUCTION

Calcium ion (Ca^{2+}) is a ubiquitous intracellular messenger that has a crucial role in determining a plethora of cellular functions such as proliferation, migration, differentiation, and communication, and mammalian cells express numerous intrinsic mechanisms responding to various extrinsic signals with specific increases in the cytosolic Ca^{2+} level ($[Ca^{2+}]_c$) and forming diverse cellular Ca^{2+} signatures with distinct spatial and temporal dynamics [1]. ATP has been recognized as one of such extrinsic signals to raise the $[Ca^{2+}]_c$ via activating multiple plasma membrane P2X and P2Y receptors [2–6]. ATP binding to the P2X receptors opens Ca^{2+}-permeable channels mediating extracellular Ca^{2+} influx. ATP can also elevate the $[Ca^{2+}]_c$ via $G_{\alpha,q/11}$-protein-coupled P2Y receptors, and more specifically, activation of the $P2Y_1$, $P2Y_2$, and $P2Y_{11}$ receptors in human cells stimulates phospholipase C-β (PLC-β) to generate inositol-1,4,5-triphosphate (IP_3), which in turn activates the IP_3 receptor and induces Ca^{2+} release from the endoplasmic reticulum (ER). Reduction in the ER Ca^{2+} level can further induce store-operated Ca^{2+} entry through the Ca^{2+} release-activated Ca^{2+} (CRAC)

[a]School of Biomedical Sciences, Faculty of Biological Sciences, University of Leeds, Leeds, United Kingdom; [b]Department of Oral Biology, Faculty of Medicine and Health, University of Leeds, Leeds, United Kingdom; [c]Inserm UMR 1069, University of Tours, Tours, France; [d]Faculty of Life Science, University of Manchester, Manchester, United Kingdom; [e]School of Molecular and Cellular Biology, Faculty of Biological Sciences, University of Leeds, Leeds, United Kingdom; [f]Department of Physiology and Neurobiology, Xinxiang Medical University, Xinxiang, People's Republic of China

Correspondence: Lin-Hua Jiang, Ph.D., School of Biomedical Sciences, Faculty of Biological Sciences, University of Leeds, Leeds LS2 9JT, U.K. Telephone: (+)44 (0)113 3434231; E-mail: l.h.jiang@leeds.ac.uk

Received September 19, 2015; accepted for publication March 14, 2016; first published online in STEM CELLS *EXPRESS* April 1, 2016.

1066-5099/2016/$30.00/0

http://dx.doi.org/10.1002/stem.2370

channels [7, 8]. Mesenchymal stem cells (MSCs) exhibit an ability to differentiate into osteoblasts, adipocytes, and chondrocytes [9–11]. These multipotent stem cells are readily isolated from various tissues, including bone marrow (BM-MSCs), adipose tissues (AT-MSCs), and dental pulp (DP-MSCs) and have been extensively explored as promising cell sources for therapeutic applications such as tissue regeneration and cell-based therapies in addition to being used in understanding tissue homeostasis [12–16]. Accumulating evidence shows that MSCs release ATP constitutively or in response to mechanical stimulation [17–20]. Previous studies consistently demonstrated that ATP induced robust Ca^{2+} responses but reported expression of a bewildering variety of P2X and P2Y receptors in MSCs from different tissues and species [17–28] and, as a result, the cognate intrinsic mechanisms remains contentious. There is also evidence for occurrence of store-operated Ca^{2+} entry in BM-MSCs [17], but the molecular identity of the Ca^{2+} channels is still elusive. Several recent studies show that ATP significantly regulates MSC differentiation, although there are striking disparities in the findings and the proposed underlying mechanisms [20, 23, 24, 27]. MSCs are highly promising in cell-based therapies for challenging clinical conditions including cardiac infarction and neurodegenerative diseases and, once transplanted into the damaged or diseased tissues or organs, MSCs are anticipated to migrate into the recipient's tissue, and the poor homing capability is a critical factor limiting the effectiveness of in vitro expanded MSC cultures in clinical applications. How MSC migration is regulated is largely unknown. Therefore, this study examined the intrinsic mechanisms for ATP-induced Ca^{2+} signaling and their roles in the regulation of cell migration in human DP-MSCs (hDP-MSCs). Our results provide strong evidence to support the purinergic P2X7, $P2Y_1$, and $P2Y_{11}$ receptors and identify the store-operated Orai1/Stim1 channel as important molecular mechanisms underlying ATP-induced Ca^{2+} signaling and further show that activation of these mechanisms stimulates cell migration in hDP-MSCs.

Materials and Methods

Chemicals and Culture Media

All general chemicals, including pyridoxal-phosphate-6-azophenyl-2′,4′-disulfonic acid (PPADS), 2-aminoethoxydiphenyl borate (2-APB), and thapsigargin (TG), were purchased from Sigma-Aldrich (U.K., http://www.sigmaaldrich.com). AZ1164373, 5-(3-bromophenyl)−1,3-dihydro-2H-benzofuro-[3,2-e]-1,4-diazepin-2-one (5-BDBD), and CGS15943 from Tocris Bioscience (U.K.). Phosphate-buffered saline (PBS), Dulbecco's modified Eagle's medium (DMEM), OPTI-MEM, fetal bovine serum (FBS), penicillin-streptomycin, trypsin-EDTA, pluronic acid F-127, and SYBR Green I were from Invitrogen (Carlsbad, CA, http://www.invitrogen.com), and collagenase P from Worthington Biochem (Lakewood, NJ, http://www.worthington-biochem.com/).

Cell Isolation and Characterization

All the experiments described below were carried out at room temperature, unless indicated otherwise. MSCs used for the vast majority of experiments were isolated from the molar teeth of three female donors (D1–D3: 9, 21, and 32 years old, respectively) and MSCs in a small number of experiments from 20 years old male donor, provided by the Leeds Dental Institute Dental Clinic. The procedures were approved by the Dental Research Ethics Committee of University of Leeds (280211/LJ/60). In brief, the pulp tissues were removed from the pulp chamber, minced into small pieces in 2 ml PBS containing 5 mg/ml collagenase P, and incubated in a humidified tissue culture incubator at 37°C and 5% CO_2 for 45–60 minutes, with gentle pipetting every 15 minutes until the tissues were totally dispersed. After addition of 7 ml DMEM with 10% FBS, cells were collected by centrifugation (∼168*g*), re-suspended in 5 ml DMEM supplemented with 20% FBS, 2 mM L-glutamine, 100 units/ml penicillin, and 100 μg/ml streptomycin, and filtered using a 70-μm cell strainer. Cells were seeded in a T25 (25-cm^2) tissue culture plastic flask and incubated in a humidified tissue incubator at 37°C and 5% CO_2 with the media changed every 3–4 days until reaching approximately 80% confluence. Cells were passaged using standard culture protocols and seeded in T25 or T75 (75-cm^2) flasks at a density of 1×10^4 cells per cm^2. Cells were used up to five passages.

Expression of the MSC positive and negative cell surface protein markers was examined by flow cytometry using a FACSCalibur (BD Biosciences, San Diego, http://www.bdbiosciences.com). Cells were suspended in flow cytometry staining buffer (PBS containing 0.5% bovine serum albumin (BSA) and 2 mM EDTA) at 1×10^7 cells per ml before treated with Fc receptor blocking solutions (TruStain FcXTM, Biolegend) for 10 minutes, and 1×10^6 cells were incubated at 4°C for 30 minutes with the following mouse anti-human antibodies: CD105-fluorescein isothiocyanate (FITC), CD90-FITC, CD73-phycoerythrin (PE), CD45-FITC, CD34-FITC, CD14-FITC, control-FITC, control-PE (Biolegend), and mouse anti-STRO-1 antibody (Santa Cruz Biotechnology, Santa Cruz, CA, http://www.scbt.com). Cells labeled with the anti-STRO-1 antibody were further incubated with FITC-conjugated goat anti-mouse IgG antibody (Invitrogen) at 4°C for 30 minutes. After washing, cells were collected by centrifugation (∼168*g*) and resuspended in 400 μl flow cytometry staining buffer. Ten thousand events were recorded for each sample, and the data were analyzed with Cell Quest software (BD Biosciences).

For osteogenic differentiation, cells were seeded into 24-well plates at 4×10^4 cells per well and cultured in basal medium (BM) for 48 hours and then in BM or osteogenic medium (OM: 100 nM dexamethasone and 50 μM ascorbate-2-phosphate in BM) for 2 weeks, with the media replaced every 3 days. The expression of alkaline phosphatase was examined under a light microscope after cells were fixed in ethanol at 4°C for 10 minutes and stained with 4% α-naphthol in water containing 24 mg/ml Fast violet B salt for 1 hour. For adipogenic differentiation, cells were seeded onto type I collagen-coated coverslips (BD Biosciences) placed in 24-well plates at 4×10^4 cells per well and cultured in BM for 48 hours before they were cultured in BM or adipogenic medium (AM: 0.5 mM isobutylmethylxanthine, 10 μM dexamethasone, 10 μg/ml insulin (Invitrogen), and 200 μM indomethacin in BM) for 3 weeks, with the media replaced every 3 days. Cells were fixed with 4% paraformaldehyde for 30 minutes and stained with 0.3% oil red O for 15 minutes and then with Harris hematoxylin for 2 minutes. Adipocytes were identified with oil red O staining. Chondrogenesis was examined in three-dimensional cell pellet cultures. Cell pellets, composed of 1×10^6 cells for each, were cultured in BM

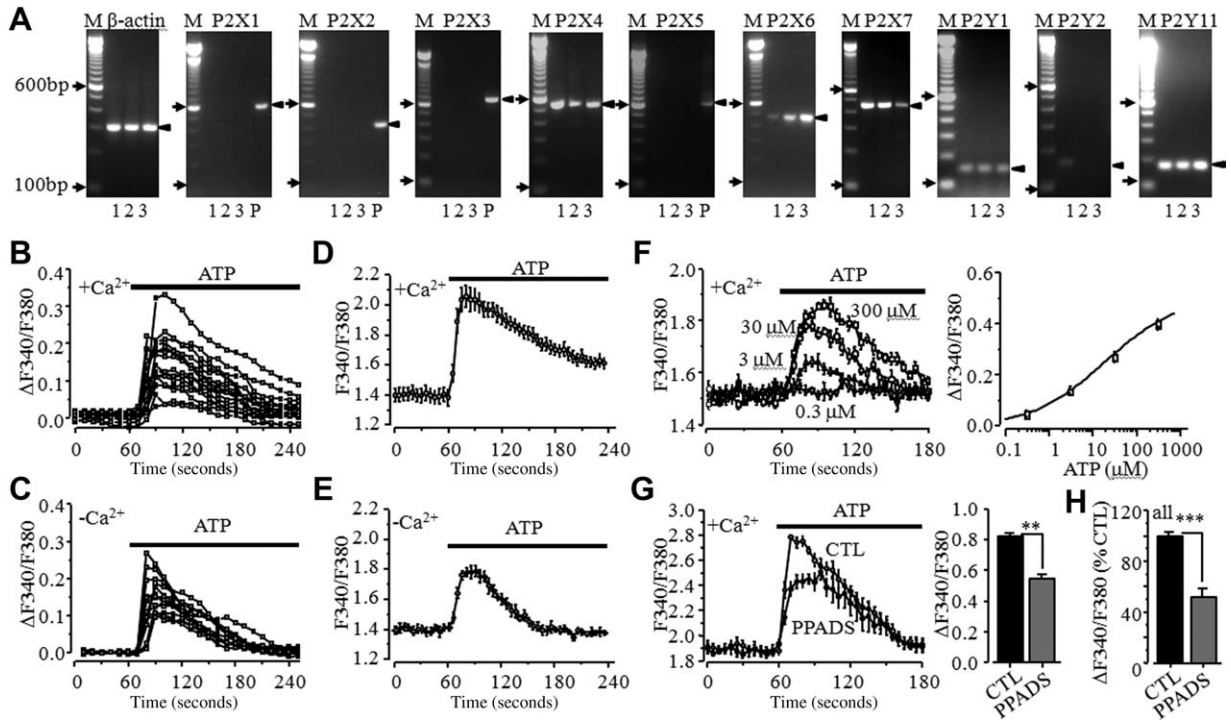

Figure 1. Profiling P2X and P2Y expression and ATP-induced Ca^{2+} responses in human dental pulp mesenchymal stem cell (hDP-MSCs). **(A)**: Reverse transcription polymerase chain reaction (RT-PCR) analysis of mRNA expression of ATP-sensitive P2X and P2Y receptors in hDP-MSCs from three donors denoted by the number (1–3). While P2X4, P2X6, P2X7, $P2Y_1$, and $P2Y_{11}$ were consistently detected, there was no expression of P2X1, P2X2, P2X3, and P2X5, and $P2Y_2$ expression was extremely low or undetectable. The two arrows on the left denote 600 bp and 100 bp DNA markers, and the arrow head on the right points to the anticipated PCR product. Plasmids (P) containing P2X1, P2X2, P2X3, or P2X5 cDNA were used as DNA templates in PCR as positive control for primers. **(B, C)**: Single cell recording of Ca^{2+} responses in individual cells to 100 μM ATP in extracellular Ca^{2+}-containing (B; 16/17 cells) and Ca^{2+}-free solutions (C; 14/15 cells). **(D, E)**: FlexStation measurement of Ca^{2+} responses to 300 μM ATP in cells in extracellular Ca^{2+}-containing (D; four wells of cells) and Ca^{2+}-free solutions (E; four wells of cells). **(F)**: Ca^{2+} responses induced by 0.3–300 μM ATP from four wells of cells for each concentration (left), and the concentration–response relationship curve with the solid line showing data fit to Hill equation with an EC_{50} of 22 μM and n_H of 0.5 (right). **(G, H)**: Summary of the inhibition of 300 μM ATP-induced Ca^{2+} responses by 10 μM PPADS in cells from the first donor (G; four wells of cells), and the mean % inhibition for three donors (H; 20 wells of cells in five independent experiments). **, $p < .001$; ***, $p < .005$. Abbreviations: CTL, control; PPADS, pyridoxal-phosphate-6-azophenyl-2′,4′-disulfonic acid.

for 48 hours by gentle shaking and then in BM or chondrogenic medium (0.1 μM dexamethasone, 10 ng/ml Transforming growth factor (TGF)-β3, 50 μg/ml ascorbic acid 2-phosphate, 1.0 mg/ml recombinant human insulin, 0.55 mg/ml human transferrin, and 0.5 μg/ml sodium selenite in BM) for 3 weeks with the media changed every 3 days. Cell pellets were paraffin embedded, sectioned, and stained with Alcian blue and Sirius red [29].

Reverse Transcriptase Polymerase Chain Reaction

Total RNA was extracted from one T75 flask of cells for each condition using TRI reagents and treated with RQ1 RNase-free DNase enzyme (Ambion, Austin, TX, http://www.ambion.com). The Ribogreen assay was carried out to determine the RNA concentrations. RNA was reverse-transcribed into cDNA using High Capacity RNA-to-cDNA Master Mix (Applied Biosystems, Foster City, CA, http://www.appliedbiosystems.com) using a Mastercycler Gradient PCR machine (Eppendorf) at 25°C for 5 minutes, 42°C for 30 minutes, and 85°C for 5 minutes. The cDNA samples were amplified using PCR and primers specific to the target genes in 5 μl reaction volume containing 0.5 μl cDNA sample, 0.6 μl 4 mM $MgCl_2$, 0.5 μl SYBR Green (Applied Biosystems), 0.25 μl 0.5 μM forward primer and 0.25 μl 0.5 μM reverse primer. The primer sequences were described in our previous studies [30, 31] and/or are available upon request. The polymerase chain reaction (PCR) protocols consist of 95°C for 10 minutes, 45 cycles of 95°C for 10 seconds, 60°C (for P2X and P2Y) or 55°C (for Orai1 and Stim) for 6 seconds and 72°C for 16 seconds, followed by a final melting step from 65°C to 95°C. The minimal cycle threshold values (C_t) were calculated from each of the quadruplicate reactions and the mean was obtained. The expression level of the gene under investigation was normalized to that of β-actin based on $2^{-[(Ct,\text{target gene} - Ct,\beta\text{-actin})]}$ [32]. The difference in the target gene expression in cells transfected with siRNA relative to that in cells transfected with scrambled siRNA was calculated using $2^{-\Delta\Delta Ct}$ method, where $\Delta\Delta C_t = (C_{t,\text{target gene}} - C_{t,\beta\text{-actin}})_{\text{siRNA}} - (C_{t,\text{target gene}} - C_{t,\beta\text{-actin}})_{\text{control}}$ [33]. The PCR products were analyzed by electrophoresis on 2% agarose gels, alongside with 100 bp DNA standards, and gel images were captured with a Biorad Gel Doc System.

Immunocytochemistry

Cells were seeded on coverslips with 15,000–20,000 per coverslip, placed in 24-well microplates, and incubated in a humidified tissue incubator at 37°C and 5% CO_2 for 24 hours prior to immunostaining. Cells were fixed with 4% paraformaldehyde for 30 minutes. After wishing with PBS three times, cells were incubated in blocking solution (PBS containing 0.2%

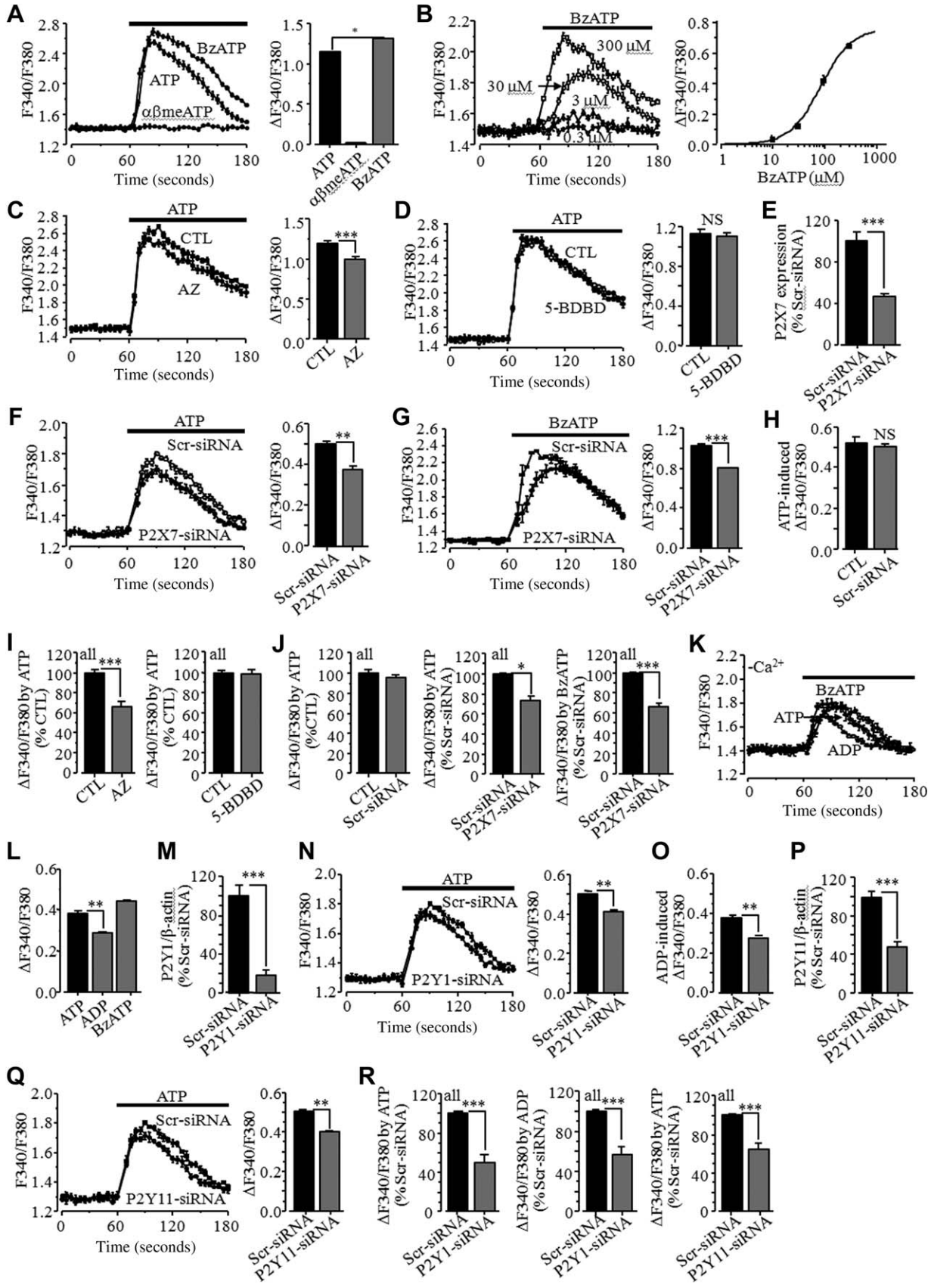

Figure 2.

Triton X-100 and 5% goat serum or BSA) for 2 hours. Primary rabbit antibodies were diluted into the blocking solution at 1:50–100 for anti-P2X7, and 1:100 for anti-$P2Y_1$ and anti-$P2Y_{11}$ (all from Alomone Labs), and cells were incubated further at 4°C for 24 hours. After washing with PBS containing 0.5% Tween-20 three times, cells were incubated in the blocking solution containing FITC-conjugated goat anti-rabbit IgG antibody at 1:1,000 (Sigma) at room temperature for 1.5 hours. After washing with PBS and rinsing with water, the coverslips were mounted on glass slides with DAPI-containing anti-fade mounting agent (Molecular Probes, Eugene, OR, http://probes.invitrogen.com) and kept at 4°C overnight before images were captured using a LSM700 confocal microscope and ZEN software (Zeiss).

Measurement of the $[Ca^{2+}]_c$

The $[Ca^{2+}]_c$ was monitored using single cell imaging and FlexStation, as described in our previous studies [34–36]. Cells were seeded on type I collagen-coated coverslips placed in 24-well plates at a 2×10^3 cells per cm^2 for single cell imaging or in 96-well assay plates at 4×10^4 cells per well for FlexStation. Cells were loaded with 4 μM Fura-2/AM (Molecular Probes) and 0.4% pluronic acid F-127 in standard Ca^{2+}-containing bath solution (SBS: 147 mM NaCl, 2 mM KCl, 1.5 mM $CaCl_2$, 1 mM $MgCl_2$, 10 mM HEPES, and 13 mM glucose 13, pH 7.3) at 37°C for 1 hour, and after washing, incubated in SBS at 37°C for 30 minutes. Cells were washed again and replaced with fresh SBS or Ca^{2+}-free solution (147 mM NaCl, 2 mM KCl, 1 mM $MgCl_2$, 1.147 mM EDTA, 10 mM HEPES, and 13 mM glucose, pH 7.3). For single cell imaging, a coverslip with cells was placed in a recording chamber under an Axiovert S100 TV fluorescent microscope (Zeiss). Cells were perfused with SBS or Ca^{2+}-free solutions. The fluorescence intensity from selected single cells was imaged every 10 seconds. Cells were perfused with indicated extracellular solutions for 60 seconds to establish the baseline before adding agonist. The fluorescence intensity from a small collection of cells was measured every 5–10 seconds using FlexStation II or III and Softmax Pro (Molecular Devices, Union City, CA, http://www.moleculardevices.com). Agonists were added after 60 seconds to establish the baseline. The $[Ca^{2+}]_c$ was monitored by the ratio of the fluorescence intensity at 510 nm excited alternatively by 340 nm and 380 nm (F_{340}/F_{380}). Data analysis was carried out using OriginPro 8.0. The agonist concentration–response curves (Figs. 1F, 2B) were least squared fit to Hill equation: $\Delta F_{340}/F_{380} = \Delta F_{340}/F_{380max}/(1 + (EC_{50}/[agonist])^{nH})$, where $\Delta F_{340}/F_{380}$ is agonist-induced change in F_{340}/F_{380}, $\Delta F_{340}/F_{380max}$ is the maximal change, EC_{50} is the agonist concentration evoking half of the maximal change, and n_H is Hill coefficient. In experiments studying the store-operated Ca^{2+} entry (Figs. 3B–3D, 4C, 4D), cells were pretreated with 1 μM TG for 30 minutes in Ca^{2+}-free solutions. TG-evoked store-operated Ca^{2+} entry was determined by the difference between the Ca^{2+} responses in TG-treated cells (+TG) and matched TG-untreated cells (−TG).

Cell Migration Assays

Cell migration was assessed using the wound healing and trans-well migration assays. For the wound healing assay, cells were seeded in 96-well plates at 4×10^5 cells per well and cultured for 48 hours to form confluent monolayers. The wound was introduced across the well by removing the cells using a 96-pin WoundMaker (Essen BioScience). Cell migration was monitored by measuring the average wound width narrowing every hour using Incucyte (Essen BioScience). Cell migration was also estimated by staining cells with SYBR Green, imaging two wound areas in each well using IncuCyte, counting the number of cells migrating into the wound area, corrected by the cell density in adjacent healthy area in the same well. The trans-well migration

Figure 2. P2X7, $P2Y_1$, and $P2Y_{11}$ receptors participate in ATP-induced Ca^{2+} responses in human dental pulp mesenchymal stem cell (hDP-MSCs). **(A)**: Ca^{2+} responses to 300 μM ATP, 300 μM BzATP, or 100 μM αβmeATP (left), and summary of the peak Ca^{2+} responses (right) in four wells of cells from the first donor. There was no discernible αβmeATP-induced Ca^{2+} response. Similar results were observed in cells from other two donors. **(B)**: Ca^{2+} responses induced by 0.3–300 μM BzATP from four wells of cells for each concentration (left), and the concentration–response relationship curve, with the solid line showing the data fit to Hill equation with an EC_{50} of 87 μM and n_H of 1.4 (right). **(C, D)**: ATP-induced Ca^{2+} responses (left) and summary of 300 μM ATP-induced peak Ca^{2+} responses (right) in control cells and cells treated with 1 μM AZ11645373 (AZ) (C) or treated with 10 μM 5-BDBD (5-(3-bromophenyl)−1,3-dihydro-2H-benzofuro-[3,2-e]-1,4-diazepin-2-one) (D), with four wells of cells from the first donor for each case. **(E)**: Quantitative reverse transcription polymerase chain reaction (RT-PCR) analysis of P2X7 mRNA expression in cells transfected with P2X7-siRNA, presented as % of that in cells with Scr-siRNA, from three wells of cells from the second and third donors each. **(F, G)**: Ca^{2+} responses (left) induced by 300 μM ATP (F) or 300 μM BzATP (G), and summary of the peak Ca^{2+} responses (right) in cells treated with Scr-siRNA or P2X7-siRNA, from four wells of cells from the first donor. **(H)**: Summary of 300 μM ATP-induced peak Ca^{2+} responses in untransfected cells and cells transfected with Scr-siRNA, from four wells of cells from the first donor. **(I)**: Summary of the mean % reduction in 300 μM ATP-induced peak Ca^{2+} responses by 1 μM AZ11645373 (left; 12 wells of cells) or with 10 μM 5-BDBD (right; 12 wells of cells) for three donors. **(J)**: Summary of the mean % reduction in the peak Ca^{2+} responses induced by 300 μM ATP or BzATP in control cells and cells transfected with Scr-siRNA (left; 12 wells of cells), and cells transfected with Scr-siRNA and P2X7-siRNA (middle and right; 12 wells of cells in each case) for three donors. **(K, L)**: Ca^{2+} responses to 100 μM ATP, 100 μM BzATP, or 100 μM ADP (K) and summary of the peak Ca^{2+} responses induced by ATP, BzATP, or ADP from four wells of cells from the first donor (L). Similar results were observed in other two donors. **(M)**: Quantitative RT-PCR analysis of the $P2Y_1$ mRNA expression in cells transfected with $P2Y_1$-siRNA, from three wells of cells for the second and third donors each. The results are presented as mean % of that in cells transfected with Scr-siRNA. **(N, O)**: Ca^{2+} responses induced by 100 μM ATP (left), and summary of peak Ca^{2+} responses induced by ATP (right) (N) and 100 μM ADP (O) in cells treated with Scr-siRNA or $P2Y_1$-siRNA, from four wells of cells from the first donor in each case. **(P)**: Quantitative RT-PCR analysis of the $P2Y_{11}$ mRNA expression in cells transfected with $P2Y_{11}$-siRNA, from three well of cells for the second and third donors each. The results are presented as mean % of that in cells transfected with Scr-siRNA. **(Q)**: Ca^{2+} responses (left), and summary of the peak Ca^{2+} responses induced by 100 μM ATP (right) in cells treated with Scr-siRNA or $P2Y_{11}$-siRNA, from four well of cells from the first donor in each case. **(R)**: Summary of the mean % reduction in ATP or ADP-induced peak Ca^{2+} responses in cells from three donors that were transfected with siRNAs. 12 wells from 3 independent experiments were used in each case. NS, no significant difference; *, $p < .05$; **, $p < .001$; ***, $p < .005$. Abbreviations: AZ, AZ11634737; CTL, control; Scr-siRNA, scrambled siRNA.

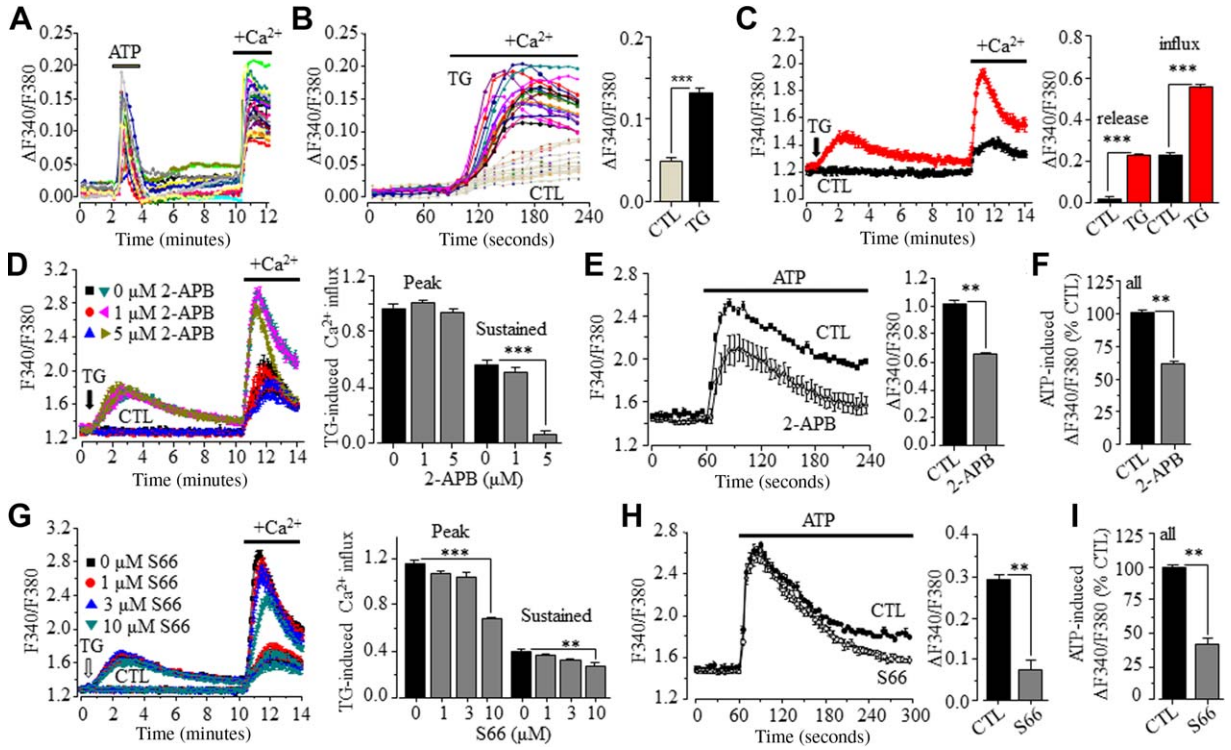

Figure 3. Store-operated Ca^{2+} entry contributes to ATP-induced Ca^{2+} responses in human dental pulp mesenchymal stem cell (hDP-MSCs). **(A)**: Single cell imaging of internal Ca^{2+} release in individual cells (19/19 cells) induced by 100 μM ATP in extracellular Ca^{2+}-free solutions, and subsequent Ca^{2+} influx upon addition of extracellular Ca^{2+}-containing solutions. **(B)**: Single cell imaging of extracellular Ca^{2+} influx upon addition of extracellular Ca^{2+}-containing solutions in control cells (CTL; 15/15 cells) or cells pretreated with 1 μM TG (18/18 cells) in extracellular Ca^{2+}-free solutions. **(C)**: FlexStation measurement of internal Ca^{2+} release in control cells (CTL) or cells treated with 1 μM TG in extracellular Ca^{2+}-free solutions, and subsequent Ca^{2+} influx upon addition of extracellular Ca^{2+}-containing solutions (left), and summary of internal Ca^{2+} release and extracellular Ca^{2+} influx in control and TG-treated cells (right). **(D)**: TG-induced internal Ca^{2+} release in extracellular Ca^{2+}-free solutions, and subsequent Ca^{2+} influx upon addition of extracellular Ca^{2+}-containing solutions in control cells (CTL) or cells treated with 1 μM and 5 μM 2-APB (left), and summary of TG-induced peak and sustained store-operated Ca^{2+} entry (right). Data were from 12 wells of cells from the first donor in 3 independent experiments. **(E)**: ATP-induced Ca^{2+} responses (left), and summary of peak Ca^{2+} responses in control cells (CTL) and cells treated with 5 μM 2-APB, from four wells of cells in each case. **(F)**: Summary of the mean % inhibition of ATP-induced peak Ca^{2+} responses by 2-APB in 12 wells of cells for each case from three donors. **(G)**: TG-induced internal Ca^{2+} release in extracellular Ca^{2+}-free solutions, and subsequent Ca^{2+} influx upon addition of extracellular Ca^{2+}-containing solutions in control cells (CTL) or cells, pretreated with 1, 3, and 10 μM synta-66 (S66) (left), and summary of TG-induced peak and sustained store-operated Ca^{2+} entry (right). Data were from 12 wells of cells from the first donor in three independent experiments. **(H)**: ATP-induced Ca^{2+} responses (left), and summary of peak Ca^{2+} responses in control cells (CTL) and cells treated with 10 μM S66, from four wells of cells in each case. **(I)**: Summary of the mean % inhibition of ATP-induced peak Ca^{2+} responses by S66 in 12 wells of cells for each case from three donors. **, $p < .001$; ***, $p < .005$. Abbreviations: 2-APB, 2-aminoethoxydiphenyl borate; CTL, control; S66, syntax66; TG, thapsigargin.

assays were carried out in 24-well plates receiving polyethylene terephthalate membrane cell culture inserts containing trans-well pores of 8 μm in diameter (BD Biosciences). The upper compartment was seeded with 5×10^4 cells, and both the upper and lower compartments were filled with DMEM with 10% FBS. ATP was added into the lower compartment. After incubation at 37°C and 5% CO_2 for 6 or 18 hours, cells attached to the side of the inserts facing the lower compartment were stained with 0.1% crystal violet prepared in 20% methanol and 80% distilled water for cell migration at 6 hours and Hoechst (5 ng/ml) for cell migration at 18 hours; cells in three to five different areas of the inserts were imaged using an IX51 microscope and Cell^F imaging system (Olympus) or a fluorescent microscope EVOS® Cell Imaging System (Zeiss). The stained cells with a size that was discernibly greater than the size of the pore were counted. For meaningful comparisons between separate experiments, relative cell migration was expressed by % of that in the absence of ATP.

Treatments with Agonists and Antagonists

In single cell imaging and FlexStation measurements of the $[Ca^{2+}]_c$, cells were exposed to ATP or other agonists during recordings. In some experiments, cells were pretreated with PPADS, 5-BDBD, 2-APB, AZ11645373, and TG during last 30 minutes incubation. In cell migration assays, antagonist was added in culture medium 30 minutes before addition of ATP.

Transfection with siRNA

Cells were seeded in 96-well plates for measurements of the $[Ca^{2+}]_c$ and cell migration, and in six-well plates for measurements of the gene expression using reverse transcriptase polymerase chain reaction (RT-PCR) at the cell densities described above. After 24 hours incubation, cells were transfected with siRNAs directed against target gene or scrambled small

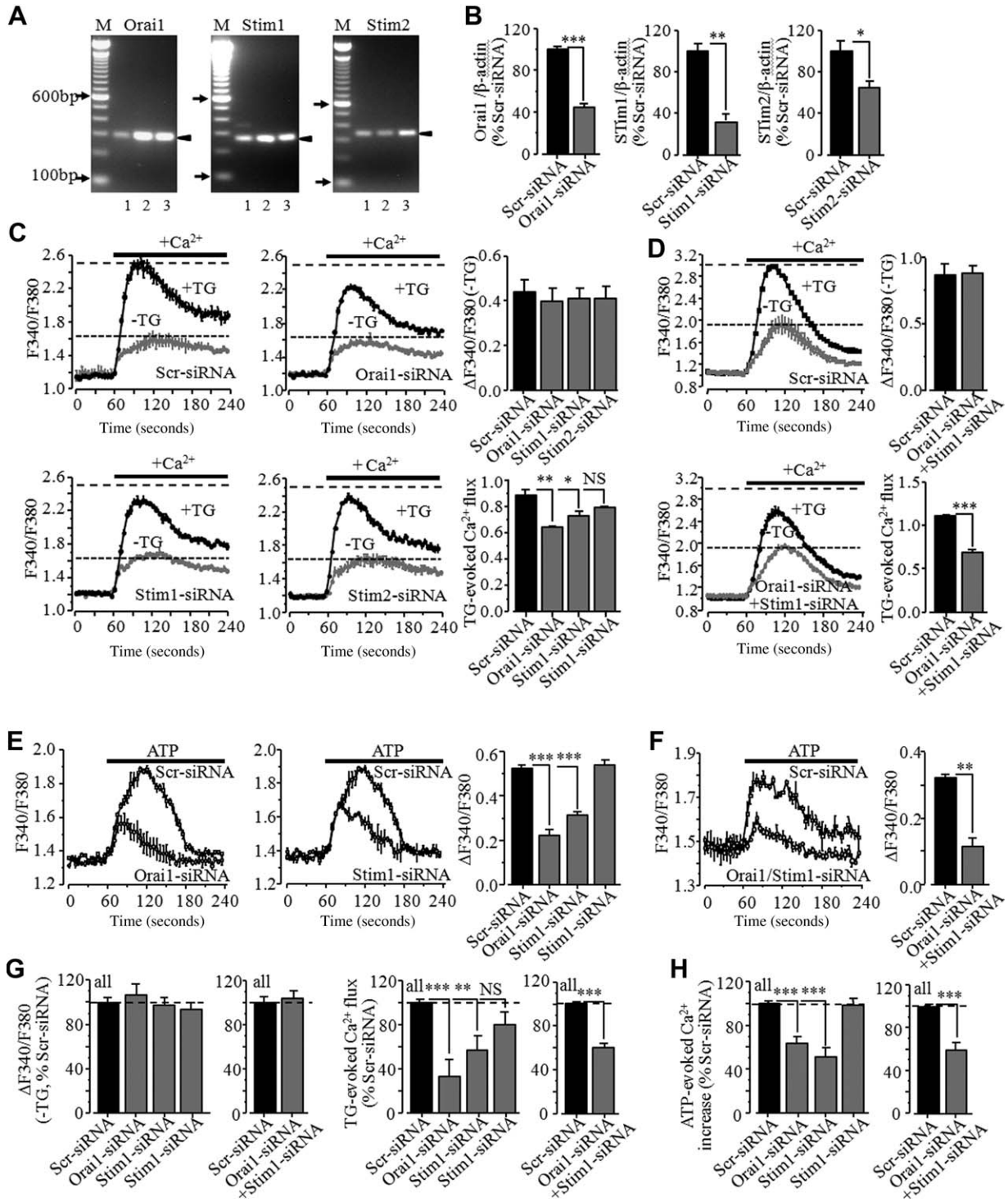

Figure 4. Orai and Stim1 mediate store-operated Ca^{2+} entry and contribute in ATP-induced Ca^{2+} responses in human dental pulp mesenchymal stem cell (hDP-MSCs). **(A)**: Reverse transcription polymerase chain reaction (RT-PCR) analysis of mRNA expression of Orai1, Stim1, and Stim2 in hDP-MSCs from three donors. The two arrows on the left in each panel denote 600 bp and 100 bp DNA markers, and the arrow head on the right points to the anticipated PCR product. **(B)**: Quantitative RT-PCR analysis of Orai1, Stim1, or Stim2 mRNA expression in cells transfected with indicated siRNA, presented as mean % of that in cells transfected with Scr-siRNA, from three well of cells for the second and third donors each. **(C)**: Extracellular Ca^{2+} influx in control cells (−TG) or TG-treated cells (+TG) transfected with indicated siRNA (left), and summary of constitutive Ca^{2+} influx (right and top) and TG-induced store-operated Ca^{2+} entry (right bottom), from four wells of cells from the first donor for each case. **(D)**: Extracellular Ca^{2+} influx in control cells (−TG) or TG-treated cells (+TG) transfected with indicated siRNA (left), and summary of constitutive Ca^{2+} influx (right top) and TG-induced store-operated Ca^{2+} entry (right bottom), from four wells of cells from the first donor for each case. The dotted and broken lines (C, D) show the Ca^{2+} responses in TG-untreated and TG-induced cells transfected with Sci-siRNA. **(E)**: ATP-induced Ca^{2+} responses in extracellular Ca^{2+}-containing solutions (left), and summary of ATP-induced peak Ca^{2+} responses (right) in cells transfected with indicated siRNA, from four wells of cells from the first donor for each case. **(F)**: ATP-induced Ca^{2+} responses in extracellular Ca^{2+}-containing solutions (left), and summary of ATP-induced peak Ca^{2+} responses (right) in cells transfected with indicated siRNA in four wells of cells from the first donor for each case. **(G)**: Summary of the peak Ca^{2+} responses in TG-untreated cells (left) and store-operated Ca^{2+} entry in TG-treated cells (right) transfected with indicated siRNA, presented as mean % of that in cells transfected with Scr-siRNA for three donors, in 12 wells of cells for each case. **(H)**: Summary of ATP-induced peak Ca^{2+} responses in cells transfected with indicated siRNA as mean % of that in cells transfected with Scr-siRNA for three donors in 12 wells of cells for each case. NS, no significant difference; *, $p < .05$; **, $p < .001$; ***, $p < .005$. Abbreviations: Scr-siRNA, scrambled siRNA; TG, thapsigargin.

interference RNA (siRNA) (Scr-siRNA), provided by Ambion. The specificity was verified by the vendor and our previous studies [31]. For each transfection, 4 μl 20 μM siRNA and 4 μl Lipofectamine2000 (Invitrogen) was separately diluted in 200 μl OPTI-MEM medium and incubated for 5 minutes before they were mixed and incubated for further 20 minutes and supplemented with 1.6 ml culture media. Cells in each well were covered with the transfection medium (100 μl for each well of 96-well plates and 1 ml for each well of 6-well plates) and cultured for 48–72 hours before use.

Data Presentation and Analysis

All data are presented as mean ± SEM, where appropriately. Figures show representative data from cells from the first donor and also show the mean data from the first three donors. Statistical analysis was carried out using Student's *t* test to compare two groups or one-way ANOVA with Tukey post hoc test to compare more than two groups by Origin software, with $p < .05$ being indicative of significance.

Results

P2X7, $P2Y_1$, and $P2Y_{11}$ Receptors Participate in ATP-Induced Ca^{2+} Signaling

Cells used in this study exhibited the characteristics proposed for MSCs [11], namely, they were adherent to plastic surface, displayed fibroblast-like morphology, and underwent osteogenic, adipogenic and chondrogenic differentiation under defined inducing conditions (Supporting Information Fig. 1). These cells also showed expression of MSC positive markers, CD73, CD90, CD105, and Stro-1, and lack of hematopoietic and endothelial cell markers, CD14, CD34, and CD45 (Supporting Information Fig. 2).

To characterize the expression of ATP-induced Ca^{2+} signaling mechanisms in hDP-MSCs, RT-PCR was firstly used to analyze the expression of ATP-sensitive purinergic P2 receptors, P2X1-7, $P2Y_1$, $P2Y_2$, and $P2Y_{11}$. In cells from the three donors examined, the mRNA transcript was detected for P2X4, P2X6, and P2X7, but not for P2X1, P2X2, P2X3, and P2X5 (Fig. 1A). Among the three ATP-sensitive P2Y receptors, the mRNA expression of $P2Y_1$ and $P2Y_{11}$ was readily detected, whereas the $P2Y_2$ expression was extremely low or undetectable (Fig. 1A). As introduced above, activation of the ATP-sensitive P2X and P2Y receptors induces extracellular Ca^{2+} influx and intracellular Ca^{2+} release respectively, leading to increases in the $[Ca^{2+}]_c$. Therefore, to determine their functional expression, ATP-induced increase in the $[Ca^{2+}]_c$ was measured using fura-2 based ratiometry. Single cell imaging showed that individual cells responded to 100 μM ATP with strong, albeit various, increases in the $[Ca^{2+}]_c$ in extracellular Ca^{2+}-containing solutions (Fig. 1B). ATP also induced salient Ca^{2+} responses in extracellular Ca^{2+}-free solution (Fig. 1C), indicating internal Ca^{2+} release and expression of functional P2Y receptors. ATP-induced Ca^{2+} responses in Ca^{2+}-containing solution last noticeably longer, suggesting that ATP induces extracellular Ca^{2+} influx in addition to internal Ca^{2+} release. Measurements using FlexStation recorded similar Ca^{2+} responses from a group of cells in extracellular Ca^{2+}-containing and Ca^{2+}-free solutions (Fig. 1D, 1E). Construction of ATP concentration-Ca^{2+} response relationship curve and fitting to Hill equation yielded an EC_{50} of 22 μM and n_H of 0.5 (Fig. 1F). ATP-induced increases in the $[Ca^{2+}]_c$ in extracellular Ca^{2+}-containing solutions were reduced by 10 μM PPADS, a generic P2 antagonist (Fig. 1G, 1H), and almost completely abolished by 30 μM PPADS (Supporting Information Fig. 3a, 3c). These results provide initial but clear evidence to confirm the expression of functional P2 receptors as the cognate Ca^{2+} signaling mechanisms to respond to extracellular ATP in MSCs.

Consistent with lack of the P2X1, P2X3, or P2X5 mRNA expression, 100 μM αβmeATP induced no discernible Ca^{2+} response (Fig. 2A), indicating lack of functional P2X receptors containing any of these subunits, at which αβmeATP is known as a potent agonist [6]. In contrast, 300 μM BzATP evoked a greater increase in the $[Ca^{2+}]_c$ than 300 μM ATP (Fig. 2A), indicating that BzATP is more potent than ATP. Construction and fitting of BzATP concentration-Ca^{2+} response relationship curve yielded an EC_{50} of 87 μM and n_H of 1.4 (Fig. 2B). ATP-induced increase in the $[Ca^{2+}]_c$ was significantly reduced by 1 μM AZ11645373 (Fig. 2C), a human P2X7 selective antagonist [37]. In contrast, ATP-induced Ca^{2+} response was completely insensitive to 10 μM 5-BDBD (Fig. 2D), a P2X4 specific antagonist with submicromolar potency [38], indicating lack of functional P2X4 receptor. Transfection of hDP-MSCs with P2X7-siRNA led to significant reduction in the P2X7 expression (Fig. 2E) and the Ca^{2+} responses induced by both BzATP and ATP (Fig. 2F, 2G), whereas transfection with scrambled siRNA (Scr-siRNA) resulted in no detectable inhibition (Fig. 2H; Supporting Information Fig. 4). The greater potency of BzATP over ATP and the sensitivity of Ca^{2+} responses induced by ATP and BzATP to inhibition by AZ11645373 and P2X7-siRNA were consistently observed in cells from three donors examined (Fig. 2I, 2J). These results provide compelling evidence to support the expression of functional P2X7 receptor.

ATP induced substantial increases in the $[Ca^{2+}]_c$ in extracellular Ca^{2+}-free solutions (Fig. 1C, 1E; Supporting Information Fig. 3c). Such ATP-induced Ca^{2+} responses were almost completely abolished by 30 μM PPADS (Supporting Information Fig. 3b, 3c). These results indicate functional expression of ATP-sensitive PLC-IP_3-coupled P2Y receptors. To further elaborate the P2Y receptors, internal Ca^{2+} release induced by P2Y subtype-preferring agonists was determined in extracellular Ca^{2+}-free solution. ADP, an agonist at $P2Y_1$, and BzATP, an agonist at $P2Y_1$ and $P2Y_{11}$, both applied at 100 μM, evoked substantial Ca^{2+} release, albeit with variable amplitudes (Fig. 2K, 2I). Moreover, knockdown of the $P2Y_1$ expression (Fig. 2M) attenuated the increases in the $[Ca^{2+}]_c$ induced by ATP (Fig. 2N) and ADP (Fig. 2O) in extracellular Ca^{2+}-containing solution. Similarly, knockdown of the $P2Y_{11}$ expression (Fig. 2P) diminished ATP-induced increase in the $[Ca^{2+}]_c$ in extracellular Ca^{2+}-containing solution (Fig. 2Q). These results, even though bearing some variations, were consistently observed in cells from the three donors examined (Fig. 2R), and therefore strongly support participation of the $P2Y_1$ and $P2Y_{11}$ receptors in ATP-induced Ca^{2+} signaling.

To provide further supporting evidence, immunofluorescence confocal microscopy was used to examine protein expression of the P2X7, $P2Y_1$, and $P2Y_{11}$ receptors. There were strong immunoreactivities in cells labeled with the antibody recognizing the P2X7, $P2Y_1$, or $P2Y_{11}$ receptor, respectively (Supporting Information Fig. 5). Taken together, the results described above provide consistent evidence to show

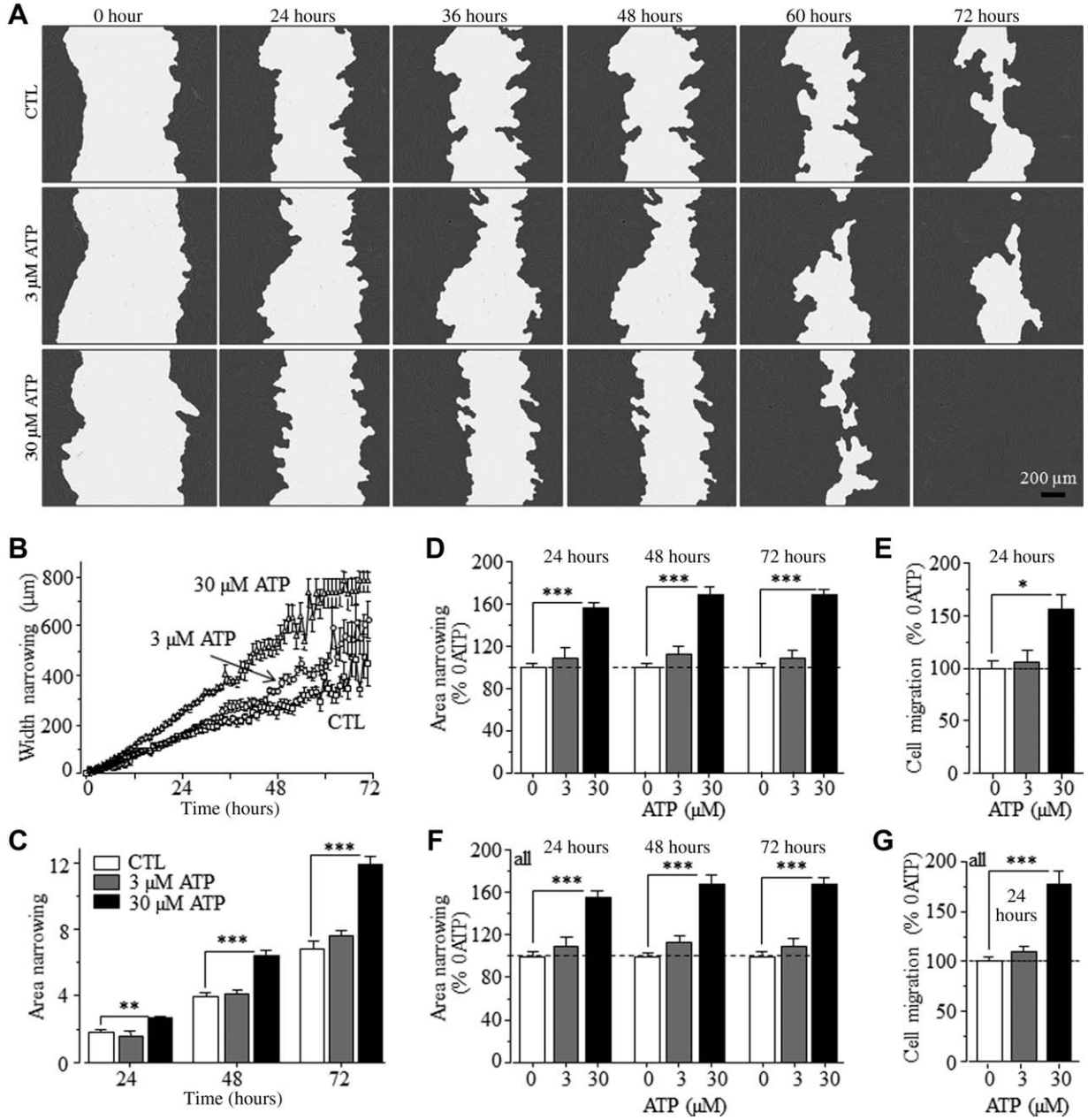

Figure 5. Extracellular ATP stimulates human dental pulp mesenchymal stem cell migration. **(A)**: Representative images showing the wound area at indicated time points during 72 hours in culture medium without (CTL) or with 3 μM and 30 μM ATP. **(B)**: The time course of wound width narrowing in the absence (CTL) and presence of ATP, from five wells of cells from the first donor for each case. **(C, D)**: Analysis of wound area narrowing at 24, 36, and 48 hours (C) and expressed as % of that under control conditions (no ATP) (D). **(E)**: Number of cells migrating to the wound area over 24 hours, expressed as % of that under control conditions (no ATP), from seven wells of cells from the first donor. **(F, G)**: Summary of the mean wound area narrowing (15 wells of cells in 3 independent experiments) (F) and cell migration (17 wells in 3 independent experiments) (G), presented as % of that under control conditions for three donors. *, $p < .05$; **, $p < .001$; ***, $p < .005$. Abbreviation: CTL, control.

that the P2X7, $P2Y_1$, and $P2Y_{11}$ receptors participate in mediating ATP-induced Ca^{2+} signaling in hDP-MSCs.

Orai1/Stim1-Mediated Store-Operated Ca^{2+} Entry Contributes in ATP-Induced Signaling

Internal Ca^{2+} release following activation of the $P2Y_1$ and $P2Y_{11}$ receptors reduces the ER Ca^{2+} level and therefore is anticipated to induce subsequent store-operated Ca^{2+} entry. Indeed, single cell imaging showed that ATP-induced internal Ca^{2+} release in extracellular Ca^{2+}-free solution led to massive Ca^{2+} influx upon Ca^{2+} add-back in individual hDP-MSCs (Fig. 3A). Pretreatment with TG in extracellular Ca^{2+}-free solution to deplete the ER Ca^{2+} store and subsequent Ca^{2+} add-back, a widely used experimental paradigm to characterize store-operated Ca^{2+} entry, was used to examine the store-operated Ca^{2+} entry and its contribution to ATP-induced Ca^{2+} signaling in hDP-MSCs. Treatment with 1 μM TG induced internal Ca^{2+} release and led to robust store-operated Ca^{2+} entry, as shown by single cell

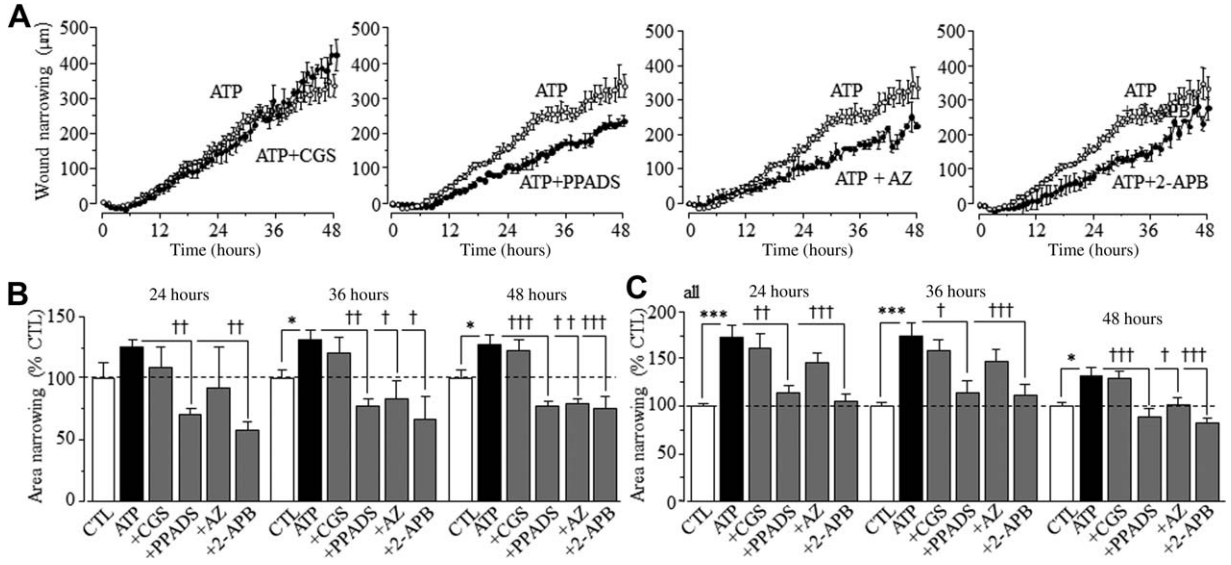

Figure 6. Pharmacological effects on ATP-induced stimulation of human dental pulp mesenchymal stem cell migration. **(A)**: Representative time course of wound width narrowing in cells with exposure to 30 μM ATP alone or together with 30 μM PPADS, 1 μM CGS15943 (CGS), 1 μM AZ11634737 (AZ), or 5 μM 2-APB, from four wells of cells from the first donor for each case. **(B)**: Analysis of wound area narrowing at 24, 36, and 48 hours for cells shown in (A), expressed as % of that in cells with ATP alone. **(C)**: Summary of the mean wound area narrowing at 24, 36, and 48 hours for three donors, expressed as % of that in cells with ATP alone, from 10–14 wells of cells from at least two independent experiments. *, $p < .05$; ***, $p < .005$, compared to control cells. †, $p < .05$; ††, $p < .01$; †††, $p < .005$, compared to cells treated with ATP alone. Abbreviations: 2-APB, 2-aminoethoxydiphenyl borate; AZ, AZ1164373; CTL, control; CGS, CGS15943; PPADS, pyridoxal-phosphate-6-azophenyl-2′,4′-disulfonic acid.

imaging (Fig. 3B) and FlexStation (Fig. 3C). In TG-untreated cells, removal of extracellular Ca^{2+} resulted in modest constitutive Ca^{2+} influx upon Ca^{2+} add-back (Fig. 4B, 4C). 2-APB is a non-selective Ca^{2+} channel inhibitor that blocks store-operated Ca^{2+} entry with an IC_{50} of approximately 10 μM but has various effects on other Ca^{2+}-permeable conductance(s) [39]. Indeed, 2-APB inhibited the constitutive Ca^{2+} flux at $\geq$10 μM and induced discernible internal Ca^{2+} release at $\geq$50 μM (Supporting Information Fig. 6). Treatment with 5 μM 2-APB reduced TG-induced store-operated Ca^{2+} entry without significant effect on TG-induced Ca^{2+} release (Fig. 3D). Application of 5 μM 2-APB suppressed both sustained and peak components of ATP-induced increases in the $[Ca^{2+}]_c$ in extracellular Ca^{2+}-containing solution (Fig. 3E), suggesting that 2-APB even at such a titrated concentration inhibits ATP-induced store-operated Ca^{2+} entry but it has additional effect. We also examined the effect of Synta66, a selective inhibitor for store-operated Ca^{2+} entry [31], on TG-induced store-operated Ca^{2+} influx and ATP-induced increases in the $[Ca^{2+}]_c$. Synta66 reduced TG-induced store-operated Ca^{2+} influx in a concentration-dependent manner (Fig. 3G) without effect on TG-induced Ca^{2+} release (Fig. 3G) or constitutive Ca^{2+} influx (Supporting Information Fig. 7). Treatment with Synta66 significantly inhibited the sustained but not the peak component of ATP-induced increases in the $[Ca^{2+}]_c$ in extracellular Ca^{2+}-containing solution (Fig. 3H). These results, albeit with some variation, were observed in cells from three donors examined (Fig. 3F, 3I), providing strong evidence to support that store-operated Ca^{2+} entry as a downstream mechanism contributes to ATP-induced Ca^{2+} signaling.

Recent studies have established that the store-operated Ca^{2+} entry in a variety of non-excitable cells is primarily mediated by the CRAC channel composed of plasma membrane pore-forming Orai1 and ER-localized Ca^{2+} sensor stromal interaction molecule 1 (Stim1) [7, 8]. There is evidence to suggest a role for the Stim1 homolog, Stim2, in the regulation of the ER Ca^{2+} level [40]. Further experiments were conducted to investigate the molecular mechanism for store-operated Ca^{2+} entry and seek molecular evidence to support contribution of store-operated Ca^{2+} entry to ATP-induced Ca^{2+} signaling in hDP-MSCs. RT-PCR analysis showed mRNA expression of Orai1, Stim1, and Stim2 in cells from the three donors examined (Fig. 4A). Transfection with Scr-siRNA resulted in no effect on TG-induced Ca^{2+} release and store-operated Ca^{2+} entry as compared to those in non-transfected cells (Supporting Information Fig. 8). Transfection with specific siRNA for Orai1, Stim1, and Stim2, as shown in our previous study [31], led to strong reduction in the expression of Orai1, Stim1, and Stim2 (Fig. 4B). Transfection with any of these siRNAs caused no effect on the constitutive Ca^{2+} influx (in grey in Fig. 4C, 4D). However, transfection with Orai1-siRNA, Stim1-siRNA but not Stim2-siRNA significantly attenuated TG-induced store-operated Ca^{2+} entry (Fig. 4C). Cotransfection with Orai1-siRNA and Stim1-siRNA inhibited TG-induced store-operated Ca^{2+} entry but there was no additive or synergistic inhibition (Fig. 4D). Consistently, knockdown of the expression of Orai1, Stim1 or both, but not Stim2, significantly reduced ATP-induced increases in the $[Ca^{2+}]_c$ in extracellular Ca^{2+}-containing solution (Fig. 4E, 4F). These results, consistently observed in cells from the three donors examined (Fig. 4G, 4H), provide the first evidence to show that Orai1 and Stim1 form the CRAC channel and further support that store-operated Ca^{2+} entry has an important role in ATP-induced Ca^{2+} signaling in MSCs.

Extracellular ATP Stimulates hDP-MSC Migration

It was unclear whether ATP regulated MSC migration and thus the wound healing assay in combination with time-lapse imaging was used to determine the effect of ATP on hDP-MSC migration. Figure 5A, 5B illustrates a set of representative

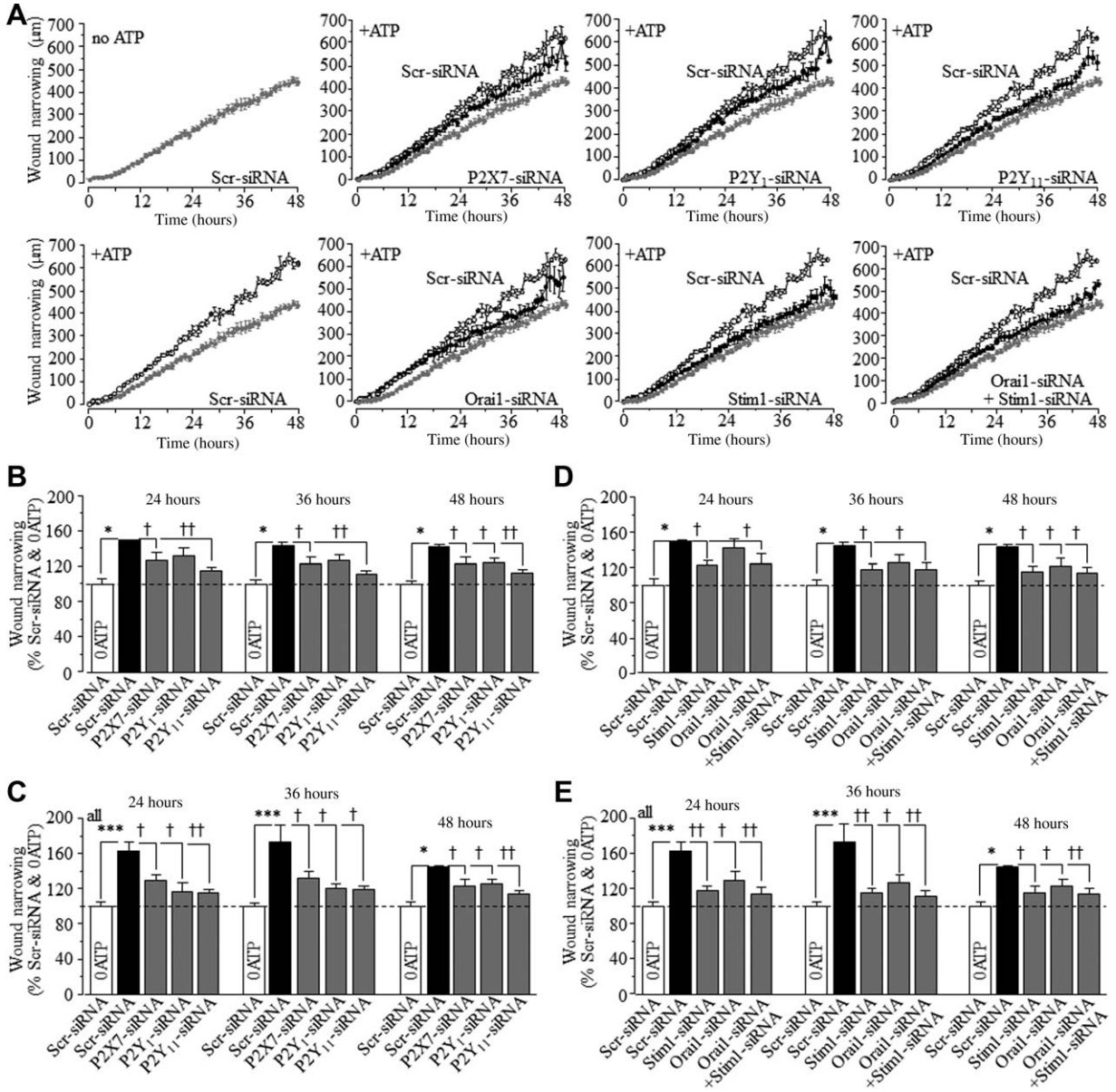

Figure 7. Genetic interventions of ATP-induced stimulation of human dental pulp mesenchymal stem cell migration. **(A)**: Representative time course of wound width narrowing in cells without (no ATP) or with exposure to 30 μM ATP (+ATP), from four wells of cells from the first donor that were transfected with indicated siRNA. The results from Scr-siRNA-transfected cells without (in grey filled symbol) or with exposure to ATP (in open symbols) were shown in the following panels for comparison. **(B–E)**: Wound area narrowing at 24, 36, and 48 hours in cells without (no ATP) or with exposure to 30 μM ATP, transfected with indicated siRNA (B) for four wells of cells from the first donor (**B**, **D**) and eight wells of cells from the first and third donors (**C**, **E**) for each case. *, $p < .05$; ***, $p < .005$, compared to control cells. †, $p < .05$; ††, $p < .01$; †††, $p < .005$, compared to control cells treated with ATP alone. Abbreviation: Scr-siRNA, scrambled siRNA.

images showing the wound areas at various time points and the corresponding time course of wound healing over 72 hours in the absence and presence of 3 and 30 μM ATP. Detailed analysis of the wound healing area at 24, 48, and 72 hours indicates that the wound healing process remained not altered by 3 μM ATP but was accelerated by approximately 50% by 30 μM ATP (Fig. 5C, 5D). Similar results were obtained by nucleus staining and counting of cells migrating into the wound area during 24 hours; the number of cells in the wound area in the presence of 3 μM ATP were similar to, but the number of cells in the wound are in the presence of 30 μM ATP significantly greater than, that under condition (Fig. 5E). These results were consistently observed in cells from three donors examined (Fig. 5F, 5G), demonstrating that ATP induces concentration-dependent stimulation of hDP-MSC migration. Trans-well chamber assay also showed that cell migration was noticeably increased after exposure to ATP for 18 hours (Supporting Information Fig. 9). It is recognized that during such relatively long exposure ATP is steadily metabolized to ADP and particularly further to adenosine, which can act on structurally and functionally distinctive adenosine receptors [41]. Increased cell migration could arise from

activation of adenosine receptors. However, ATP-induced stimulation of hDP-MSC migration was not significantly inhibited by 1 μM CGS15943, a generic adenosine receptor inhibitor with submicromolar potency [42], and by contrast completely abolished by 30 μM PPADS (Fig. 6A, 6B). These results, observed in cells from all three donors (Fig. 6C), show that ATP stimulates hDP-MSC migration predominantly via activation of the P2 receptors.

P2X7, $P2Y_1$, and $P2Y_{11}$ Receptors, and Orai1/Stim1 Channel Play a Role in Mediating ATP Stimulation of hDP-MSC Migration

Finally, the role of the above-described ATP-induced Ca^{2+} signaling mechanisms in ATP-induced stimulation of hDP-MSCs was investigated by determining the effects of pharmacological and genetic inhibition of their expression and/or function. ATP-induced stimulation of cell migration was attenuated by 1 μM AZ11645373 or 5 μM 2-APB (Fig. 6A–6C). ATP-induced stimulation of cell migration was also significantly reduced by siRNA knockdown of the expression of P2X7 or $P2Y_{11}$ receptor (Fig. 7A–7C). Moreover, ATP-induced stimulation of hDP-MSC migration was strongly inhibited by siRNA knockdown of the expression of Stim1 or both Orai1 and Stim1 (Fig. 7A, 7D, 7E). Knockdown of the $P2Y_1$ or Orai1 expression resulted in significant inhibition of ATP-induced stimulation of cell migration in hDP-MSCs, albeit the inhibition being less effective and more variable among different donors (Fig. 7B, 7C). These results overall support that the P2X7, $P2Y_1$ and $P2Y_{11}$ receptors and the Orai1/Stim1 channel play a significant role in ATP-induced stimulation of hDP-MSC migration.

Discussion

This study has made several important findings. First, the P2X7, $P2Y_1$, and $P2Y_{11}$ receptors are identified as molecular mechanisms that contribute in mediating ATP-induced Ca^{2+} signaling in hDP-MSCs. Second, the Orai1/Stim1 CRAC channel is expressed and mediates store-operated Ca^{2+} entry in hDP-MSCs and, as a downstream mechanism following activation of the P2Y receptors, participates in ATP-induced Ca^{2+} signaling. Third, ATP stimulates hDP-MSC migration, and finally, the above-described purinergic and store-operated Ca^{2+} signaling mechanisms play a significant role in mediating ATP-induced stimulation of hDP-MSC migration.

As introduced above, previous studies consistently showed that extracellular ATP induced pronounced increases in the $[Ca^{2+}]_c$ in MSCs but reported expression of a striking variety of P2X and P2Y receptors, in part due to the fact that MSCs used in previous studies were from different tissue origins or less well-defined donors. This study examined hDP-MSCs from several donors and obtained consistent evidence to demonstrate that P2X7, $P2Y_1$, and $P2Y_{11}$ are the purinergic P2 receptors responsible for ATP-induced Ca^{2+} signaling in hDP-MSCs (Figs. 1 and 2), confirming expression of these P2 receptors in MSCs reported by some previous studies using BM-MSCs and AT-MSCs [19–22, 28]. Nonetheless, this study observed noticeable variations in the results obtained in cells from different donors, for example, at both mRNA and functional expression levels (Figs. 1A, 4A). Such variations may explain to some extent the variable efforts of treating cells with the same inhibitor or siRNA on ATP-induced Ca^{2+} responses (Fig. 2R) and stimulation of cell migration (Figs. 6B, 6C, 7B–7D) that were noticed in this study, as well as the disparate results reported by previous studies. This study has provided the first evidence, as far as we are aware, to identify that Orai1 and Stim1 are expressed in hDP-MSCs and form a CRAC channel to mediate store-operated Ca^{2+} entry and, furthermore, Orai1/Stim1-mediated Ca^{2+} entry contributes to ATP-induced Ca^{2+} signaling as an important downstream mechanism following the P2Y receptor activation (Figs. (3 and 4)).

The ability of MSC differentiation along specific lineages is clearly important for tissue regeneration and replacement. Several recent studies show that ATP regulates adipogenesis and osteogenesis of hBM-MSC and hAT-MSCs, albeit with discrepancies in the reported findings and the proposed underlying mechanisms [20, 23, 24, 27]. The poor migration/homing capacity of in vitro expanded MSC cultures is critical in limiting the effectiveness of MSC-based therapies. This study using the widely used cell migration assays showed that ATP at micromolar concentrations stimulates hDP-MSC migration (Fig. 6). Furthermore, this study using pharmacological and genetic interventions provides consistent evidence to suggest that the P2X7, $P2Y_1$, and $P2Y_{11}$ receptors and the Orai1/Stim1 channel play a significant role in ATP-induced stimulation of hDP-MSC migration (Fig. 7). This is the first report describing ATP-induced stimulation of MSC migration and shedding light on the underlying mechanisms. Evidently, further efforts are required to better understand how purinergic and store-operated Ca^{2+} signals regulate cell migration and whether in vitro priming with ATP increases the homing capacity of MSC in vivo. Emerging evidence shows that extracellular magnesium influences ATP-induced Ca^{2+} signaling and mineralized matrix deposition in BM-MSC [43], and it is interesting to examine whether extracellular magnesium can affect ATP-induced regulation of MSC migration.

Conclusion

In conclusion, this study shows that purinergic P2X7, $P2Y_1$, and $P2Y_{11}$ receptors and store-operated Orai1/Stim1 channel represent the intrinsic mechanisms for ATP-induced Ca^{2+} signaling in hDP-MSCs and activation of such signaling mechanisms stimulates cell migration. Such information is useful in optimizing MSC cultures to improve the efficiency of their therapeutic applications as well as in better understanding MSC-mediated tissue homeostasis.

Acknowledgments

We are grateful to the persons who kindly donated their teeth used for cell preparations in this study. Hongsen Peng was a recipient of an international research scholarship from University of Leeds. We are grateful to Prof DJ Beech University of Leeds School of Medicine for providing synta66.

Author Contributions

H.P., X.Y., and L.-H.J.: designed the research; H.P., Y.H., and F.M.: performed the experiments; S.R., J.L., J.A.S., and S.P.:

contributed intellectual inputs into the research; L.-H.J.: wrote the manuscript; all authors contributed to discussion, and revised and approved the manuscript.

Disclosure of Potential Conflicts of Interest

The authors indicate no potential conflicts of interest.

References

1 Berridge MJ, Bootman MD, Roderick HL. Calcium signalling: Dynamics, homeostasis and remodelling. Nat Rev Mol Cell Biol 2003; 4:517–529.

2 North RA. Molecular physiology of P2X receptors. Physiol Rev 2002;82:1013–1067.

3 von Kugelgen I. Pharmacological profiles of cloned mammalian P2Y-receptor subtypes. Pharmacol Ther 2006;110:415–432.

4 von Kugelgen I, Harden TK. Molecular pharmacology, physiology, and structure of the P2Y receptors. Adv Pharmacol 2011;61:373–415.

5 Jacobson KA, Boeynaems JM. P2Y nucleotide receptors: Promise of therapeutic applications. Drug Discov Today 2010;15:570–578.

6 Jiang L.-H. P2X receptor-mediated ATP purinergic signaling in health and disease. Cell Health Cytoskeleton 2012;4:83–101.

7 Parekh AB. Store-operated CRAC channels: Function in health and disease. Nat Rev Drug Discov 2010;9:399–410.

8 Amcheslavsky A, Wood ML, Yeromin AV et al. Molecular biophysics of Orai store-operated Ca2+ channels. Biophys J 2015;108: 237–246.

9 Pittenger MF, Mackay AM, Beck SC et al. Multilineage potential of adult human mesenchymal stem cells. Science 1999;284: 143–147.

10 Zuk PA, Zhu M, Ashjian P et al. Human adipose tissue is a source of multipotent stem cells. Mol Biol Cell 2002;13:4279–4295.

11 Dominici M, Le Blanc K, Mueller I et al. Minimal criteria for defining multipotent mesenchymal stromal cells. The International Society for Cellular Therapy position statement. Cytotherapy 2006;8:315–317.

12 Caplan AI. Adult mesenchymal stem cells for tissue engineering versus regenerative medicine. J Cell Physiol 2007;213:341–347.

13 Bianco P. "Mesenchymal" stem cells. Annu Rev Cell Dev Biol 2014;30:677–704.

14 Phinney DG, Prockop DJ. Concise review: Mesenchymal stem/multipotent stromal cells: the state of transdifferentiation and modes of tissue repair—Current views. Stem Cells 2007;25:2896–2902.

15 Levi B, Longaker MT. Concise review: Adipose-derived stromal cells for skeletal regenerative medicine. Stem Cells 2011;29:576–582.

16 Fakhry M, Hamade E, Badran B et al. Molecular mechanisms of mesenchymal stem cell differentiation towards osteoblasts. World J Stem Cells 2013;5:136–148.

17 Kawano S, Otsu K, Kuruma A et al. ATP autocrine/paracrine signaling induces calcium oscillations and NFAT activation in human mesenchymal stem cells. Cell Calcium 2006; 39:313–324.

18 Coppi E, Pugliese AM, Urbani S et al. ATP modulates cell proliferation and elicits two different electrophysiological responses in human mesenchymal stem cells. Stem Cells 2007;25:1840–1849.

19 Riddle RC, Taylor AF, Rogers JR et al. ATP release mediates fluid flow-induced proliferation of human bone marrow stromal cells. J Bone Miner Res 2007;22:589–600.

20 Sun D, Junger WG, Yuan C et al. Shockwaves induce osteogenic differentiation of human mesenchymal stem cells through ATP release and activation of P2X7 receptors. Stem Cells 2013;31:1170–1180.

21 Ferrari D, Gulinelli S, Salvestrini V et al. Purinergic stimulation of human mesenchymal stem cells potentiates their chemotactic response to CXCL12 and increases the homing capacity and production of proinflammatory cytokines. Exp Hematol 2011;39:360–374, 374 e1-5.

22 Fruscione F, Scarfi S, Ferraris C et al. Regulation of human mesenchymal stem cell functions by an autocrine loop involving NAD^+ release and $P2Y_{11}$-mediated signaling. Stem Cells Dev 2011;20:1183–1198.

23 Ciciarello M, Zini R, Rossi L et al. Extracellular purines promote the differentiation of human bone marrow-derived mesenchymal stem cells to the osteogenic and adipogenic lineages. Stem Cells Dev 2013;22:1097–1111.

24 Noronha-Matos JB, Coimbra J, Sá-e-Sousa A et al., P2X7-induced zeiosis promotes osteogenic differentiation and mineralization of postmenopausal bone marrow-derived mesenchymal stem cells. FASEB J 2014;28:5208–5222.

25 Ichikawa J, Gemba H. Cell density-dependent changes in intracellular Ca^{2+} mobilization via the $P2Y_2$ receptor in rat bone marrow stromal cells. J Cell Physiol 2009;219:372–381.

26 Biver G, Wang N, Gartland A et al. Role of the $P2Y_{13}$ receptor in the differentiation of bone marrow stromal cells into osteoblasts and adipocytes. Stem Cells 2013;31: 2747–2758.

27 Zippel N, Limbach CA, Ratajski N et al. Purinergic receptors influence the differentiation of human mesenchymal stem cells. Stem Cells Dev 2012;21:884–900.

28 Faroni A, Rothwell SW, Grolla AA et al. Differentiation of adipose-derived stem cells into Schwann cell phenotype induces expression of P2X receptors that control cell death. Cell Death Dis 2013;4:e743.

29 Lee HJ, Choi BH, Min BH et al. Low-intensity ultrasound stimulation enhances chondrogenic differentiation in alginate culture of mesenchymal stem cells. Artif Organs 2006;30:707–715.

30 Jelassi B, Anchelin M, Chamouton J et al. Anthraquinone emodin inhibits human cancer cell invasiveness by antagonizing P2X7 receptors. Carcinogenesis 2013;34:1487–1496.

31 Li J, Cubbon RM, Wilson LA et al. Orai1 and CRAC channel dependence of VEGF-activated Ca2+ entry and endothelial tube formation. Circ Res 2011;108:1190–1198.

32 Zoldan J, Lytton-Jean AK, Karagiannis ED et al. Directing human embryonic stem cell differentiation by non-viral delivery of siRNA in 3D culture. Biomaterials 2011;32:7793–7800.

33 Livak KJ, Schmittgen TD. Analysis of relative gene expression data using real-time quantitative PCR and the 2(-Delta Delta C(T)) Method. Methods 2001;25:402–408.

34 Liu L, Zou J, Liu X et al. Inhibition of ATP-induced macrophage death by emodin via antagonizing P2X7 receptor. Eur J Pharmacol 2010;640:15–19.

35 Zou J, Ainscough JF, Yang W et al. A differential role of macrophage TRPM2 channels in Ca(2)(+) signaling and cell death in early responses to H(2)O(2). Am J Physiol Cell Physiol 2013;305:C61–C69.

36 Li DL, Liu X, Xia R et al. Pharmacological properties of ATP-sensitive purinergic receptors expressed in human G292 osteoblastic cells. Eur J Pharmacol 2009;617:12–16.

37 Stokes L, Jiang LH, Alcaraz L et al. Characterization of a selective and potent antagonist of human P2X(7) receptors, AZ11645373. Br J Pharmacol 2006;149:880–887.

38 Balazs B, Danko T, Kovacs G et al. Investigation of the inhibitory effects of the benzodiazepine derivative, 5-BDBD on P2X4 purinergic receptors by two complementary methods. Cell Physiol Biochem 2013;32:11–24.

39 Bootman MD, Collins TJ, Mackenzie L et al. 2-Aminoethoxydiphenyl borate (2-APB) is a reliable blocker of store-operated Ca2+ entry but an inconsistent inhibitor of InsP3-induced Ca2+ release. FASEB J 2002;16: 1145–1150.

40 Brandman O, Liou J, Park WS et al. STIM2 is a feedback regulator that stabilizes basal cytosolic and endoplasmic reticulum Ca2+ levels. Cell 2007;131:1327–1339.

41 Zimmermann H. Extracellular metabolism of ATP and other nucleotides. Naunyn Schmiedebergs Arch Pharmacol 2000;362:299–309.

42 Ghai G, Francis JE, Williams M et al. Pharmacological characterization of CGS 15943A: A novel nonxanthine adenosine antagonist. J Pharmacol Exp Ther 1987;242:784–790.

43 Zhang L, Yang C, Li J et al. High extracellular magnesium inhibits mineralized matrix deposition and modulates intracellular calcium signaling in human bone marrow-derived mesenchymal stem cells. Biochem Biophys Res Commun 2014;450:1390–1395.

See www.StemCells.com for supporting information available online.

